World Journal of Condensed Matter Physics, **2011, 1, 37-48**
doi:10.4236/wjcmp.2011.12007 Published Online May 2011 (http://www.SciRP.org/journal/wjcmp)

Dielectric Relaxation in Pure Columbite Phase of $SrNb_2O_6$ Ceramic Material: Impedance Analysis

Karuna Nidhan Singh, Parmendra Kumar Bajpai*

Department of Pure & Applied Physics, Guru Ghasidas Vishwavidyalaya, Bilaspur, India.
Email: bajpai.pk1@gmail.com

Received January 5th, 2011; revised March 24th, 2011; accepted March 26th, 2011.

ABSTRACT

Controlling the heating rate during calcination and cooling rate during sintering, pure columbite like phase of $SrNb_2O_6$ is synthesized. By optimizing the sintering temperature, ceramic with density (> 92%) *is achieved for material calcined at* 1125˚C *and sintered at* 1200˚C. *The ceramic shows orthorhombic structure with lattice parameters a* = 11.011 *Å, b* = 7.7136 *Å, c* = 5.5969 *Å having average grain size* ≈ 1.03 *μm. The temperature dependent dielectric response shows a peak at temperature* 300.9˚C, *which shows significant dielectric dispersion towards high temperature side of the peak with almost dispersion free low temperature side; an effect observed in relaxors. Dielectric dispersion in the material is fitted with the Jonscher's relation. Impedance analysis suggests strongly temperature dependent relaxation. The dielectric relaxation is polydispersive and conduction is mainly through grains. The equivalent circuit model for the impedance response is proposed and the temperature dependence of circuit elements deduced. The frequency dependent ac conductivity at different temperatures indicated that the conduction is governed through thermally activated processes. AC conduction activation energies are estimated from Arrhenius plots and conduction mechanism is discussed.*

Keywords*: *Electro Ceramics, Dielectrics, Microstructure, Sintering Optimization, Dielectric Relaxation

1. Introduction

Alkaline earth and transition metal niobate with general formula $A^{2+}Nb_2O_6$ (with A = Mg, Ca, Sr, Ba, Mn, Fe, Co, Ni, Cu, Zn, Cd, and Pb) have been widely studied [1-8]. Most of these compounds stabilize in isomorphic orthorhombic phase [9,10]. Many of them in columbite phase exhibit, excellent dielectric properties at microwave frequencies [11-13]. Moreover, these compounds are generally used as precursor materials for the synthesis of high-Q perovskite $Ba(A_{1/3}Nb_{2/3})O_3$ [14]. Microwave dielectric properties of the columbite phases are, to a large extent, sensitive to the preparation route [12,15]. However, the synthesis of single phase columbite is often difficult because of the formation of corundum-like ($A_4Nb_2O_9$) phases [15]. The properties of ceramics are greatly affected by the characteristics of the powder such as particle size, morphology, purity and chemical composition [16]. In normal solid state route, compositional homogeneity is generally not achieved. By using chemical methods, e.g. co-precipitation, sol-gel, hydrothermal and colloid emulsion techniques, one can efficiently control the morphology and chemical composition of prepared powder [17]. However, the sinterability of the material remains an issue and often in the chemical synthesis routes, the densification of materials is not reported that is important for using the materials for device purposes. Further, the earlier studies have mainly concerned about the preparation routes and detailed dielectric behavior; electrical conduction mechanism and contribution of grains and grain boundaries in dielectric relaxation are not studied. For any device application, an understanding of these properties is very much required. Therefore in this paper an attempt has been made to control the processing parameter including the oxidation of grain boundaries during cooling from high temperature while sintering the materials. To the best of our knowledge, no such detailed report exists in the literature. We, therefore, report the optimization of process parameters viz. calcination and sintering in order to prepare the $SrNb_2O_6$ in pure columbite phase with good siterability. The dielectric properties and impedance analysis of $SrNb_2O_6$ of such phase pure are investigated and reported in the paper.

2. Experimental Procedure

2.1. Sample Preparation

$SrNb_2O_6$ is synthesized by taking stoichiometric amounts

of $SrCO_3$ (Loba 99.9%), Nb_2O_5 (Loba 99.5%) using solid-state reaction route. The stoichiometric amounts of precursors were wet mixed in acetone for 12 hours. The mixed powders were calcined at 1125˚C for 6 hours in a microprocessor controlled furnace (Superheat, India) with controlled heating profile. Calcined powders were analyzed using X-ray diffraction technique (X-ray diffractometer, Rigaku-Miniflex). Fine calcined powders were pressed into cylindrical pellets of 10 mm diameter and 1-2 mm thickness under an isostatic pressure of 100 MPa. Polyvinyl alcohol (PVA) was used as a binder. The pellets were sintered at different temperatures (1150˚C, 1175˚C, 1200˚C, 1225˚C) for 6 hours and cooled down to room temperature with controlled cooling rate.

2.2. Characterization

The phase formation of the sintered pellet has been identified using x-ray diffraction analysis with CuK_α ($\lambda = 1.54056$ ***Å*****).** For dielectric measurements, the sintered samples were electroded with silver paste and heated at 500˚C for 2 hours before measurements were performed. The electrical impedance (Z), capacitance (C) and loss angle (tan) were measured in the temperature range (100 – 400˚C) and at the rate of 2˚C min-1 in the frequency range (100 Hz-1MHz) using a computer controlled LCR HI-TESTER (HIOKI-3532-50). Surface morphology of the sample is investigated using surface electron microscopy (SEM).

3. Result and Discussion

3.1. X-ray Diffraction Studies

Figure 1(a) depicts the XRD pattern of $SrNb_2O_6$ ceramic calcined at 1125˚C. From the observed interplanar spacing (dobs) of all XRD peaks, unit cell parameters were obtained using a standard XRD interpretation software POWD. The unit cell was selected for which $d = (d_{obs}-d_{cal})$ is minimized. All major X-ray reflection peaks observed could be fitted satisfactorily in orthorhombic columbite phase with lattice constants a = 11.011 Å, b = 7.7136 Å, c = 5.5969Å which matches well with reported JCPDS data (JCPDS File No. 28-1243). The powders sintered at different temperatures (1150˚C, 1175˚C, 1200˚C, 1225˚C,) were again subjected to X-ray diffraction analysis as shown in **Figure 1(b)**. Phase pure material is obtained for the sample calcined at 1125˚C and sintered at 1200˚C; the experimental density (> 92% of the theoretical one) is obtained for sintered material. The estimated density for different sintering temperatures is shown in **Table 1**. The particle size determined using Scherer formula, is estimated ≈ 413Å.

The microstructure of the sintered pellets and distribution of grains over the sample surface were studied by scanning electron micrographs. The typical SEM micrograph of $SrNb_2O_6$ is shown in **Figure 2**. Well developed homogeneously distributed and elongated spherical grains are observed. The average grain size (≈ 1.03m) is calculated using linear intercept method.

3.2. Dielectric Study

The temperature dependence of both dielectric permittivity and tangent loss (in the inset) are depicted in **Figure 3** at different frequencies (1 KHz, 5 KHz, 10 KHz, 50 KHz, 100 KHz, and 1 MHz); the values of dielectric constant increases with increase in temperature and a peak evolves at around 300˚C. The peak value of dielectric constant as well as that of tangent loss decreases (**Figure 3**) and the peak shifts towards higher temperature with increase in frequency. The increase in dielectric response with temperature may be due to interfacial polarization dominating over dipolar polarization. Observed peak also indicates the onset of some additional relaxation mechanism in the material around 300˚C. Dielectric dispersion at higher temperature side of the peak is evident in both components of dielectric permittivity.

The frequency dependence of real (ε') and imaginary (ε") part of dielectric constant on a log-log plot at different temperatures are shown in **Figure 4**. Up to 200˚C, real part of dielectric constant is higher than its imaginary part, and both values decreases with frequency. With further increase in temperature, there is a sudden rise in ε" and it starts with higher value than ε', intersecting at 3 kHz at 250˚C; intersecting frequency shift towards higher frequency as temperature increased (4 kHz at 300˚C). Higher values of both the components of dielectric constant, as temperature rises, reveal the effect of space charge polarization and/or conducting ion motion. The relatively higher values of ε" at low frequency, especially at higher temperature, suggests the free charge motion that may be related to ac conductivity relaxation, whereas the large values of ε' at lower frequencies may be associated with hopping conduction. Moreover, with increase in frequency, the ε' and ε" terms becomes almost parallel at higher temperatures. This type of behavior is reported in other conducting ion dielectrics [18] and is associated with ion hoping as the dominant mechanism of dielectric relaxation [19].

The frequency dependence of real (ε') and imaginary (ε") part of dielectric constant in the 50-400˚C temperature range on a log-log scale is shown in **figures 5(a)** and **(b)**, respectively. Both ε' and ε" show dispersions at low frequencies and gets almost saturated at higher frequencies. The dispersions increase with increase in temperature. Such dispersions in both components of complex dielectric constant are observed commonly in ferroelectrics with appreciable ionic conductivity and are referred

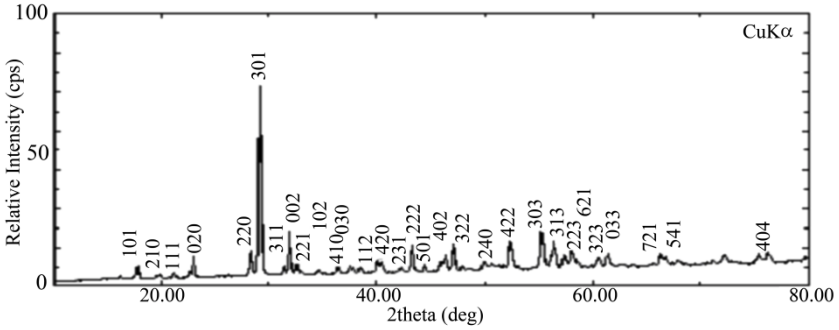

(a)

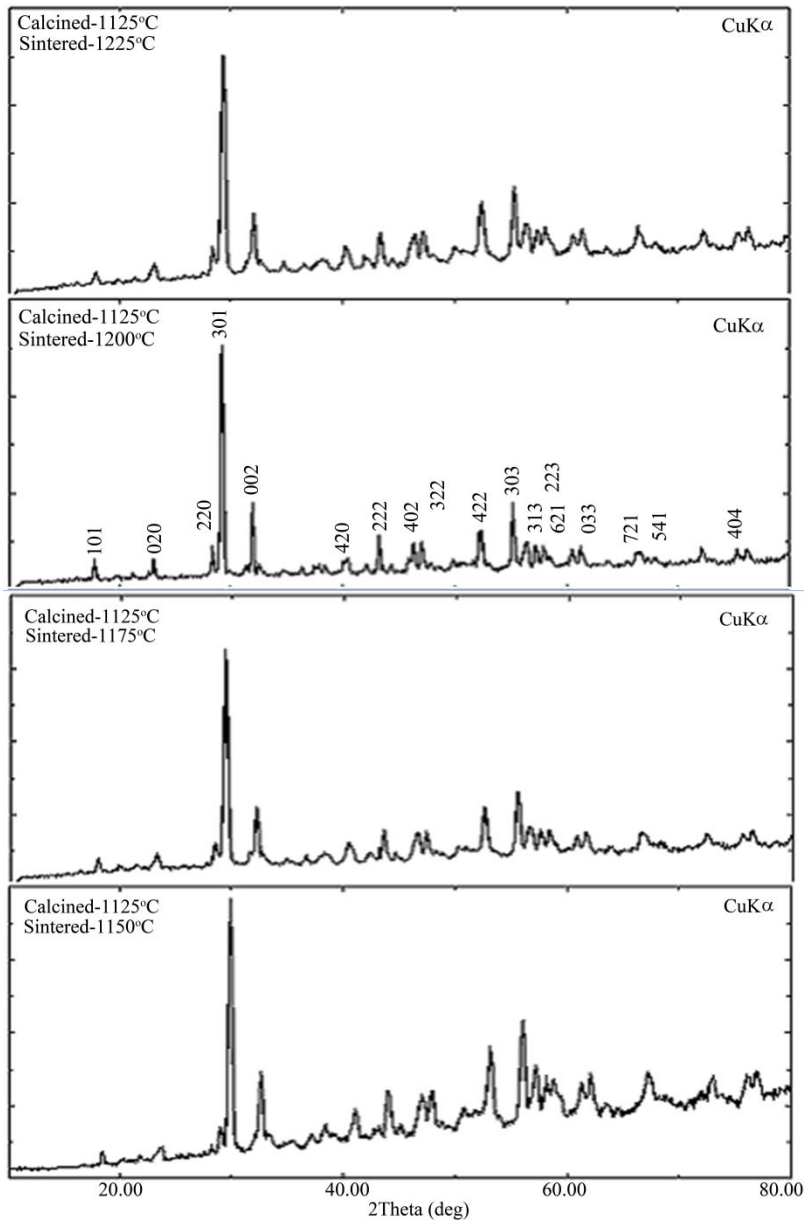

(b)

Figure 1. (a) X-ray diffraction profile of $SrNb_2O_6$ (SN); (b) X-RD pattern of pure phase $SrNb_2O_6$ at different sintering temperature.

Table 1. Structural parameters for various sintering conditions of $SrNb_2O_6$.

Composition	Crystal Structure	Unit cell parameters in (Å)			d_{expti}.gm/c.c	d_{Theo} gm/c.c	% density
		a	b	c			
Sample-I Sintered 1150˚C	Orthorhombic	11.210	7.6922	5.6254	4.329	5.523	78.38
Sample-II Sintered 1175˚C	Orthorhombic	11.124	7.7102	5.6204	4.5358	5.558	81.60
Sample-III Sintered 1200˚C	Orthorhombic	11.011	7.7136	5.5969	5.2489	5.638	92.60
Sample-IV Sintered 1225˚C	Orthorhombic	11.008	7.7198	5.6126	4.7786	5.619	85.04

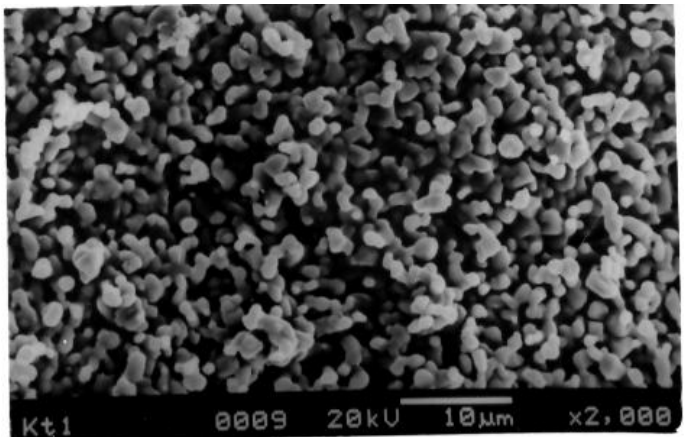

Figure 2. SEM micrograph of pure phase $SrNb_2O_6$.

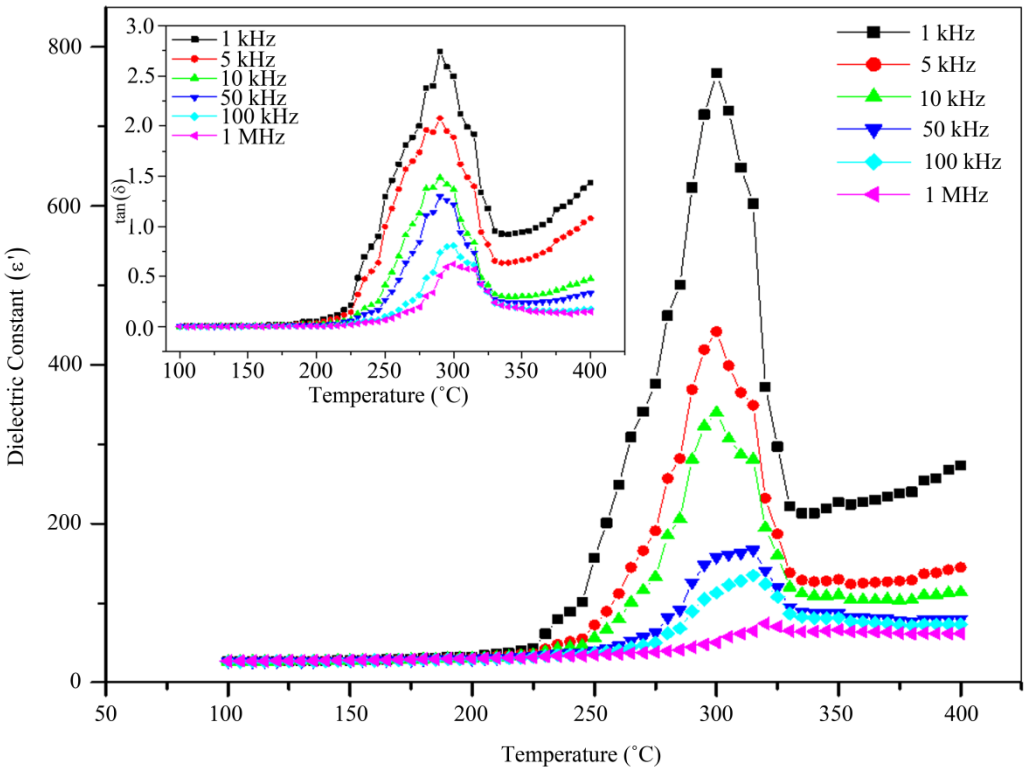

Figure 3. Temperature dependence of dielectric constant (ε'). Inset shows temperature dependence of dielectric loss.

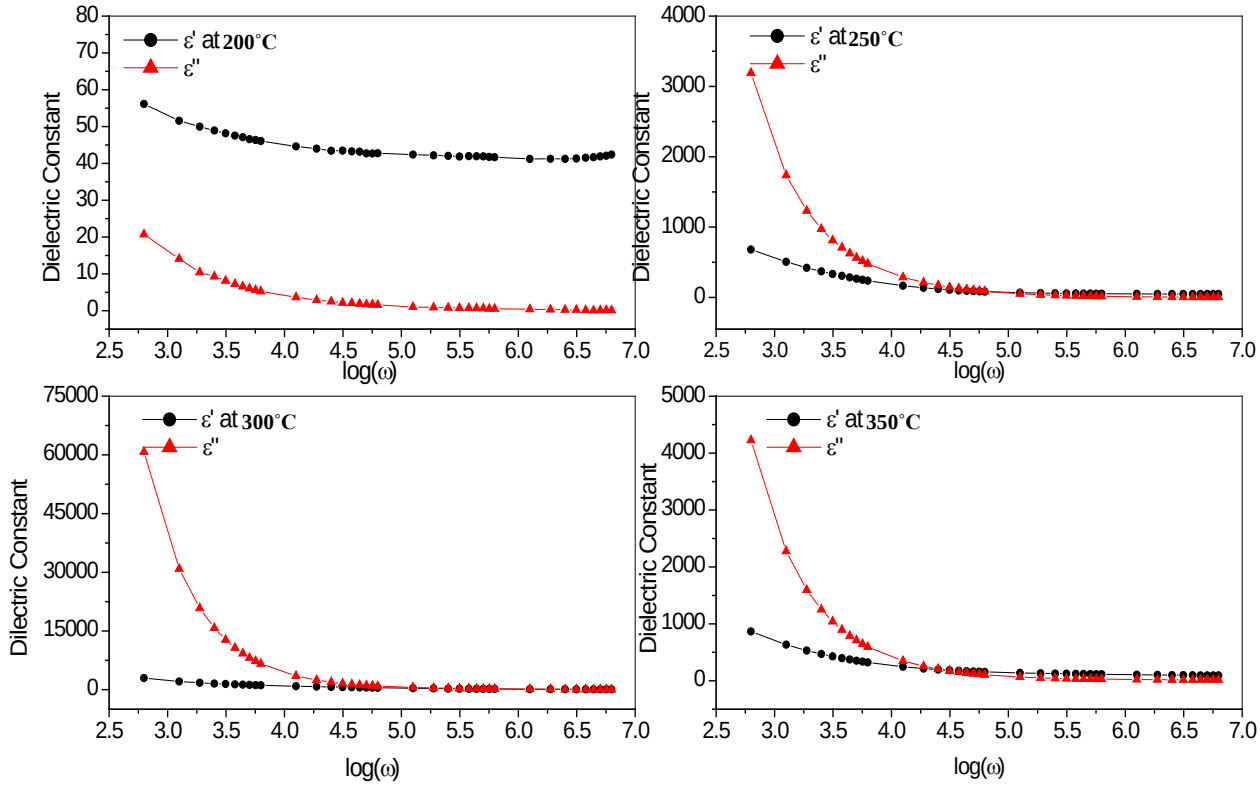

Figure 4. Comparison of dispersion in ε'' and ε' in the (200°C - 400°C) temperature range.

to as low frequency dielectric dispersion (LEDD) [20,21] and are associated with space charge accumulation effect. The complex dielectric constant as a function of the frequency ω in accordance with the Jonscher's power law [22] is

$$\varepsilon^* = \varepsilon' - \varepsilon'' = \varepsilon_\infty + \sigma/\varepsilon_0\omega + \left(a(T)/\varepsilon_0\right)\left(i\omega^{n(T)-1}\right) \quad (1)$$

where ε_∞ is the high frequency value of the dielectric constant, n(T) is the temperature dependent exponent and a(T) determines the strength of the polarizability arising from the universal mechanism in question. The real and imaginary parts of the complex dielectric constant are given as

$$\varepsilon' = \varepsilon_\infty + \sin\left(n(T)\tfrac{\pi}{2}\right)\left(a(T)/\varepsilon_0\right)\left(i\omega^{n(T)-1}\right) \quad (2)$$

$$\varepsilon'' = \sigma/\varepsilon_0\omega + \cos\left(n(T)\frac{\pi}{2}\right)\left(a(T)/\varepsilon_0\right)\left(i\omega^{n(T)-1}\right) \quad (3)$$

where the first term in Equation (2) determines the lattice response and the second term corresponds to charge career contribution to the dielectric response. Similarly, in Equation (3) the first term reflects the DC conduction contribution and the second term represents the charge career contribution to dielectric loss. At low frequencies, the contribution due to charge career term $\left(\sin\left(n(T)\tfrac{\pi}{2}\right)\left(a(T)/\varepsilon_0\right)\left(i\omega^{n(T)-1}\right)\right)$ dominates and lattice response part ε_∞ can be neglected. Therefore, Equation (2) for constant n yields a straight line with slope (n- 1). At higher frequencies, the charge careers fail to respond to the applied external field and the dielectric constant is mainly due to lattice contribution. This may account for the observed frequency dependence of dielectric constant; a linear decrease with frequency in low frequency region and frequency dependent plateau region at high frequencies. With increasing temperature, the range of frequencies in which charge career contribution dominates increase showing that charges have sufficient energy to overcome the barrier and get released. A non-linear fitting using Equations (2) and (3) give the values of parameters n (T), and a (T), as depicted in **Figure 5(c)** at different temperatures. At low temperatures, n is close to 1, showing Debye type relaxation. With increase in temperature, its value decreases showing increase in interaction and distributed relaxation at higher temperatures. The a(T) value increase slowly with temperature showing the strength of polarizability increasing. Frequency dispersion of ε" gives two slopes, -1 in the low frequency region and (n-1) in the high frequency region. With increasing temperature, the frequency range with slope -1(DC conduction) increases and at higher temperatures

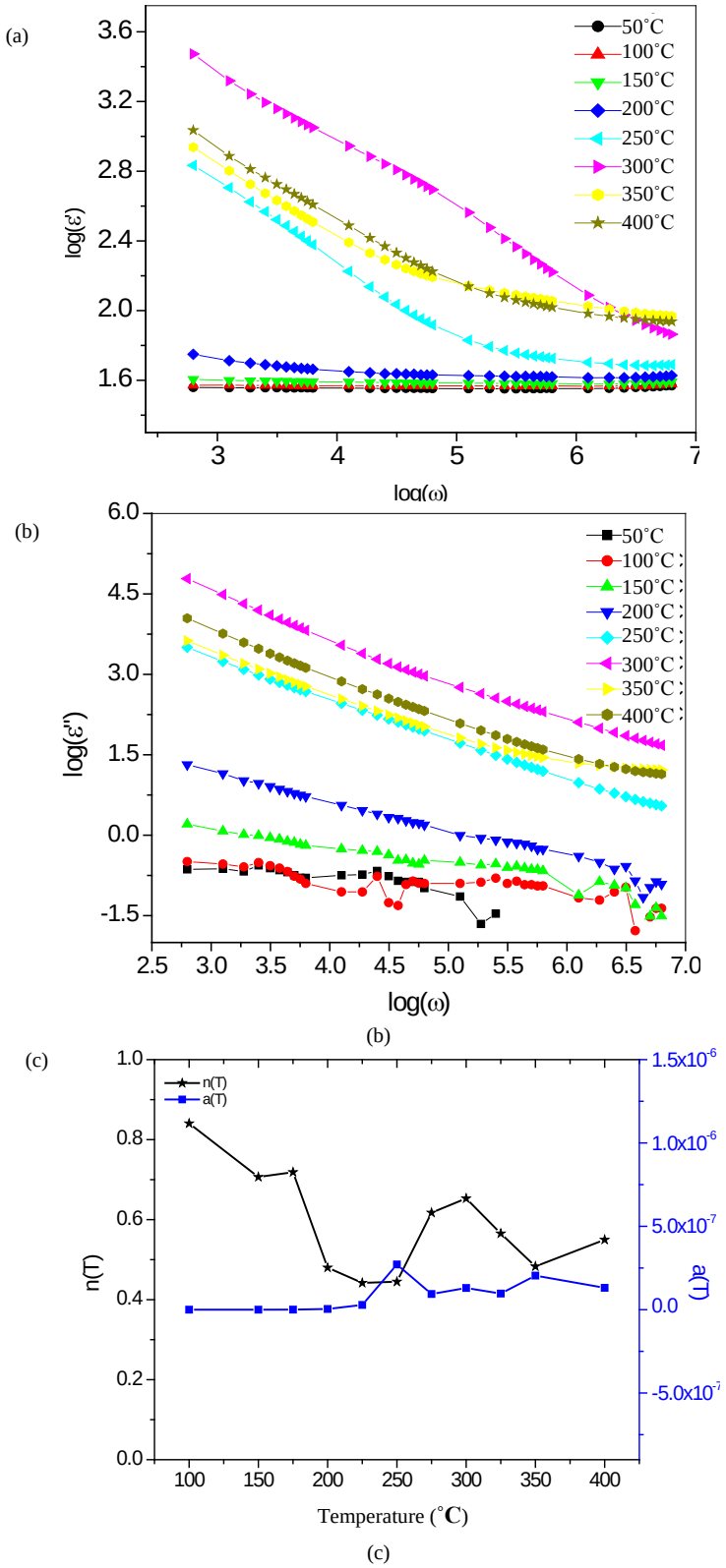

Figure 5. (a) Frequency dependence of real (ε') part of dielectric constant in the (50-400˚C) temperature range on a log-log scale. (b) Frequency dependence of imaginary (ε") part of dielectric constant in the (50-400˚C) temperature range on a log-log scale. (c) Temperature dependence of n(T) and a(T).

dc conduction dominates the charge career conduction.

3.3. Impedance Studies

The nature of the material response to an applied a.c. field and processes involved is explored by analyzing the a.c. impedance behavior. Impedance spectroscopy may be a better tool to understand the grain and grain boundary relaxation process, especially when the contribution of grains is separated from that of grain boundaries. The frequency dependence of the electrical properties of a material can be described in terms of complex impedance Z*, complex admittance Y*, the complex permittivity *, complex electric modulus M*, and the dielectric loss or the dissipation factor tan. They are related to one another [23] as follows; $\tan\delta = \varepsilon''/\varepsilon' = M''/M' = Z'/Z'' = Y'/Y''$. In case of single relaxation process, a semicircle is obtained for each admittance function when plotted in the complex plane. Spectroscopic techniques present various possibilities insofar as the representation of data is concerned. Each representation can be made use of to highlight a particular aspect of the response of a sample. Thus for instance, in as much as Z" vs. frequency plots highlight phenomena with the largest resistance, the M" plots pick out those of the smallest capacitances [23-29]. The sample is sintered at higher temperature (1125˚C), oxygen loss may occur. This may lead to the formation of barrier layers at the grain-grain boundary interface thus affecting the impedance of grains and grain boundaries [30].

Figure 6 shows the variation of the imaginary part of the impedance (Z'') as a function of frequency. Z'' plots show broad peaks at different frequencies with asymmetric broadening depending on the temperature of measurement. This would imply that the relaxation is temperature dependent, and there is apparently not a single relaxation time, and thereby relaxation process involved, but different relaxations with their own discrete relaxation times depending on the temperature. As the temperature is increased, in addition to the expected decrease in magnitude of Z'', there is a shifts in the peak frequencies towards higher frequency side. Also it is evident that with increasing temperature, there is a broadening of the peaks and at temperatures where temperature dependent dielectric response shows peak, the Z'' response is almost flat. As the temperature is increased further, Z'' response increases and then starts decreasing associated with peak broadening at increased temperature. This implies the spread of relaxation times on both sides of dielectric peak temperatures and the existence of temperature dependent electrical relaxation phenomena. Probably, high temperature triggers grain boundary relaxation process as is also evident from the asymmetric broadening of the peaks [30].The most probable relaxation time could be calculated from the loss peak in the Z'' versus frequency plots using the relation $\tau = RbCb = 1/\omega m$. From these data, the τ at various temperatures is calculated. Graph between $\ln(\omega m)$ versus 1/T is shown in inset of **Figure 6**. The τ value decreases with increasing temperature, indicating that the behavior is typical semiconductor one. Calculated activation energy for the process is 0.18 eV.

Figure 7 shows M" as a function of frequency at different temperatures (inset shows temperature dependence of ωm obtained from M" curve). It is seen that M" exhibits a symmetric maximum (M"max). The M"max shifts toward higher frequencies as the temperature is increased. At 300˚C, the electric modulus loss peak crosses the measurement windows and beyond this temperature. At further higher temperature, a more broadened peak appears that shifts towards higher frequencies with increasing the temperature. This once again supports two different relaxation processes dominating the response above and below 300˚C. Thus the dielectric response peak observed is associated with switching of relaxation process. Frequency m corresponding to M"max gives the most probable relaxation time τ_m ($\omega m\tau m = 1$). Activation energy estimated from modulus data is 0.59 eV below 300˚C and 0.32 eV above this temperature. As the modulus represents the response from the interior of grains, the activation energies for charges (defects) in the bulk are relatively more than for charges within interface region.

The complex impedance plots Z' vs. Z'' for representative temperatures is shown in **Figure 8**. The arc crosses the Z'' axis at lower values with increasing temperatures, showing that the grain resistance decreases with temperature. This could be fitted with series network R_s-(R_1Q)C_1-R_2C_2, as shown in **Figure 8**, where Q represents the constant phase element-a capacitor with universal Jonscher's type capacitance. The series resistance Rs in the model is included as the Z'' does not intersect at origin. This may be due to electrode roughness and porousness of the material. Inclusion of constant phase element is due to the fact that value of exponent n(T) in Jonscher's equation decreases up to 0.5 from 1 in dielectric response (**Figure 5(c)**). The values of parameters R_s, R_1, C_1, R_2, C_2, Q and n proposed are calculated and plotted in **Figures 9 (a)** and **(b)** as a function of temperature. The value of C_1 increases slowly with increase in temperature whereas the R_1 decreases and above the dielectric peak temperature both becomes almost constant. The behavior could be associated with the grains dominating the conduction process below 300˚C. The series resistance R_s also increases at high temperature and reached maximum at 250˚C, reflecting that the charges trapped at the bulk electrode interface are mig-

rated into the bulk. The most interesting change lies in constant phase element Q that increases with decrease in the value of n. Thus the grain boundaries start trapping free charges that is released from grains at high temperatures. The value of R_2 and C_2 remains almost temperature independent. The resistance associated with grains is much higher than those of grain boundaries below dielectric peak temperature. Therefore the dielectric peak may be associated with resistive grains becoming conductive.

3.4. Electrical Conductivity Study

The ac conductivity was calculated from the impedance data using the relation $\sigma_{ac} = \omega\varepsilon_0\varepsilon_r(\tan\delta)$. **Figure 10** shows the variation of ac conductivity with frequency at different temperatures. It is clear from the figure that the material at low frequencies exhibits dispersion. Conductivity increases with increase in temperature and frequency. The conductivity could be fitted through the expression $\sigma_{ac} = \sigma_{dc} + A\omega^n$, known as Jonsher's law [29],

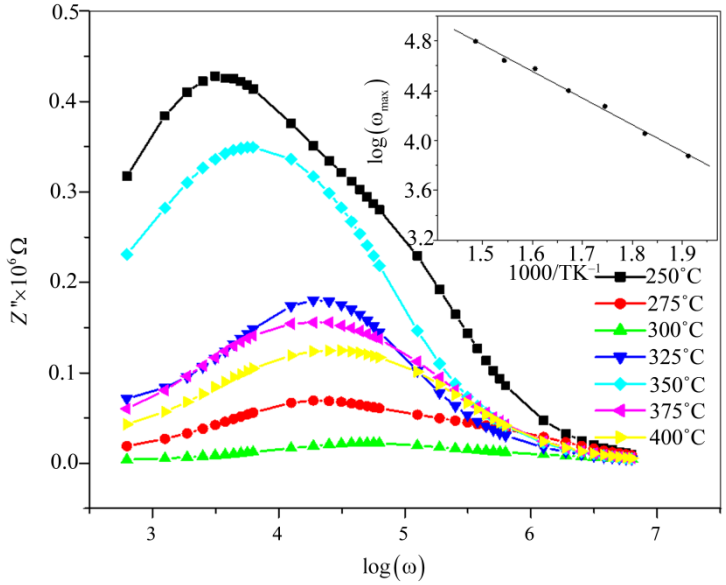

Figure 6. Frequency dependence of imaginary part of impedance (Z"). Inset shows temperature dependence of m obtained from impedance for SN.

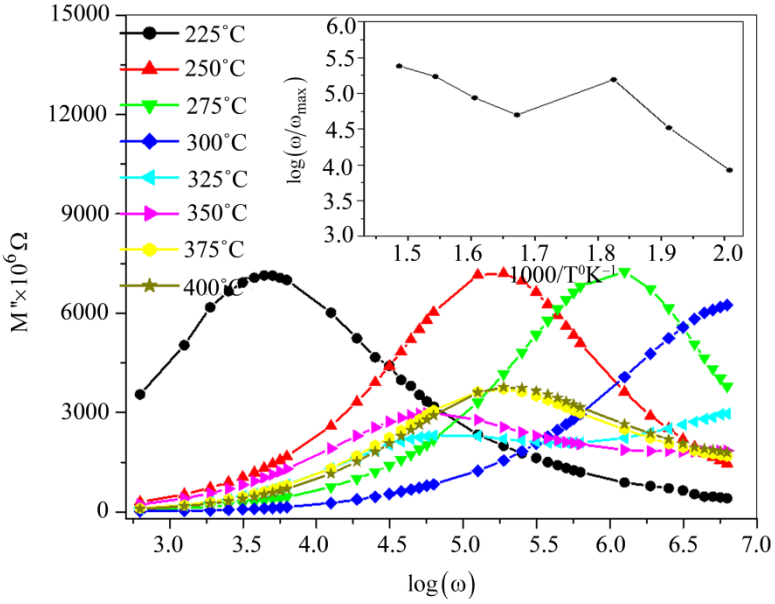

Figure 7. Imaginary part of electric modulus (M") as a function of frequencies at representative temperatures for SN.

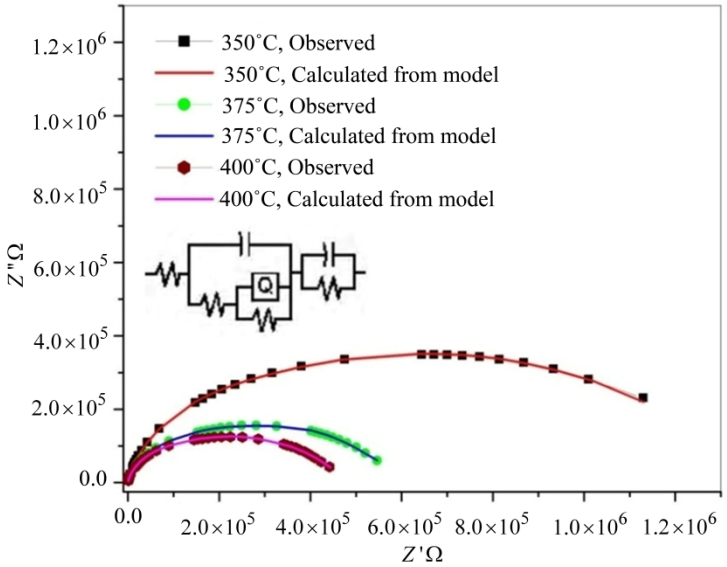

Figure 8. Complex impedance plots (Z' vs. Z") at various temperatures along with equivalent circuit fitting for the model as shown in the figure.

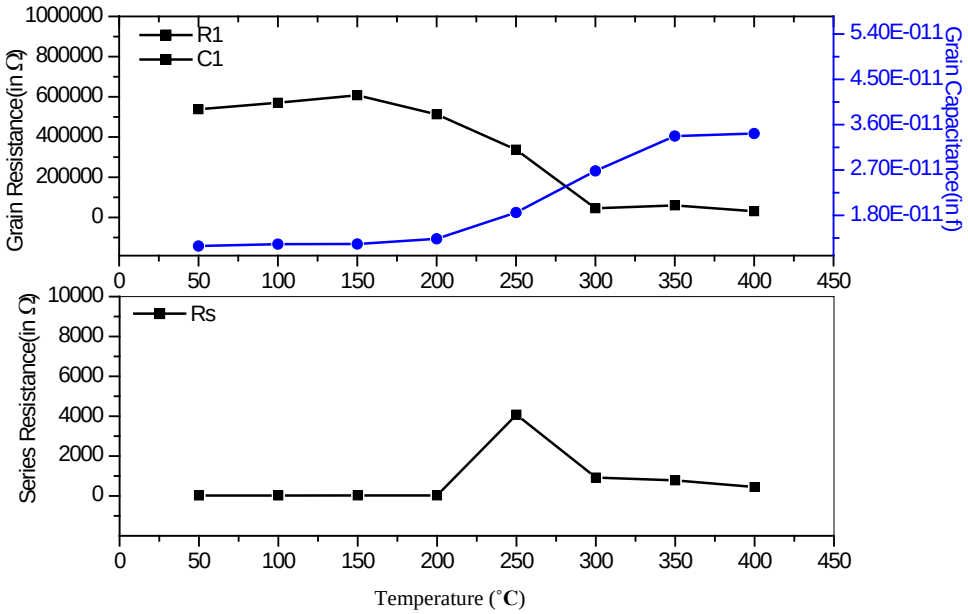

Figure 9. (a) Temperature dependence of equivalent circuit parameters (R_1, C_1, Rs) (b) Temperature dependence of equivalent circuit parameters (Q, n, R_2C_2).

where *A* is a thermally activated quantity and *n* is the frequency dependent exponent that takes values < 1. The data were fitted using the above relation and the calculated values of σ_{dc}, A and n are shown in **Table 2**. According to Jonsher, the origin of the frequency dependent conductivity lies in the relaxation phenomenon arising due to mobile charge carriers. The low frequency dispersion thus is associated with ac conductivity whereas almost frequency independent (especially at higher temperatures) conductivity at high frequencies corresponds to the dc conductivity of the material. The temperature at which the grain resistance dominates over grain boundary is marked by change in slope of conductivity with frequency. The frequency at which the slope changes is known as hopping frequency, which corresponds to polaron hopping of charges species [30-32]. As the temperature increases, the hopping frequency shifts towards lower side. Temperature dependence of AC conductivity of material is shown in **Figure 11**. The conductivity of the material is found to increase with increase in temperature indicating the NTCR (negative temperature coefficient of resistance) like semiconductors, and it is related

to the bound carriers trapped in the sample. The activation energy values at different frequencies have been calculated assuming the Arrhenius behavior and summarized in **Table 3**.

4. Conclusions

Phase pure columbite structure in SrNb2O6 is stabilized through standard solid state reaction route by controlling the processing parameters. The crystal structure is orthorhombic with unit cell parameter a = 11.011 *Å*, b = 7.7136 *Å*, c = 5.5969 *Å*. The experimental density is > 92% and average grain size is 1.03 μm. Space charge accumulation effect and free charge motion at low frequency and higher temperature is established. The dielectric dispersion results fitted with Jonscher's dielectric dispersion formalism gives coefficient a(T) and exponent n(T), which show non-Debye type relaxation due to interaction of charge careers at high temperatures. It also indicates that conducting charges and free charges both contribute to the dielectric relaxation in the material. Impedance

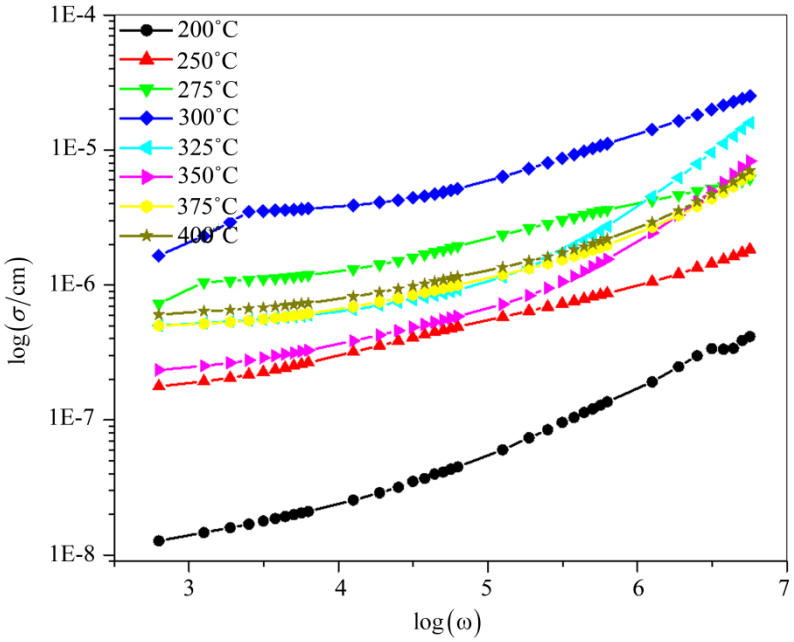

Figure 10. A.C conductivity as a function of (log) in SN.

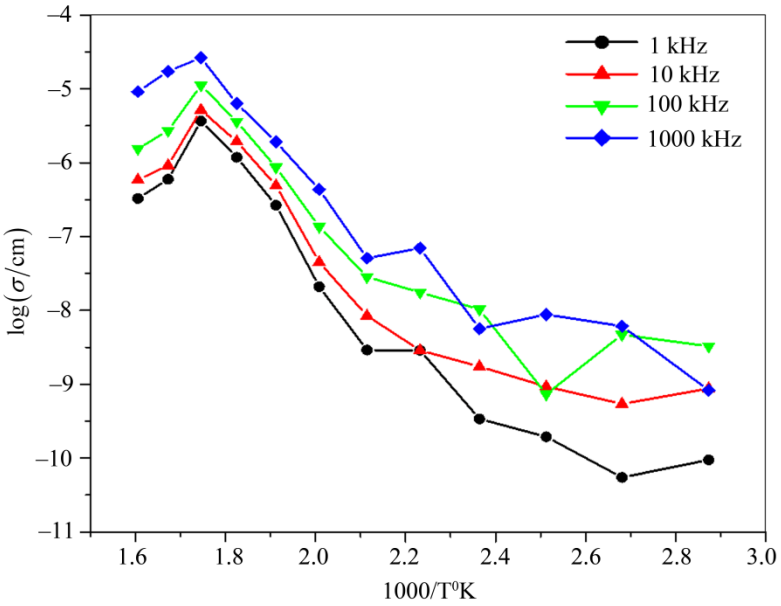

Figure 11. Arrhenius plots of AC conductivity at different frequencies.

Table 2. Calculated values of σ_{dc}, A and n by expression $\sigma_{ac} = \sigma_{dc} + A\omega^n$.

Temperature(˚C)	σ_{dc}	A	n
200	5.4203E-8	2.2404E-8	0.09656
225	2.6683E-9	1.7042E-10	0.50105
250	2.0532E-7	3.2756E-9	0.3982
275	2.7052E-7	1.7647E-7	0.23043
300	2.0637E-6	2.7393E-8	0.43341
325	6.3406E-7	1.1969E-11	0.90399
350	4.4132E-7	5.5385E-12	0.91078
375	7.4112E-7	7.7948E-11	0.72067
400	8.7604E-7	8.409E-11	0.71941

Table 3. Activation energy at different frequencies, calculated by linear fitting of temperature dependence of AC conductivity data.

Frequency in (KHz)	Temperature Range	
	Activation Energy (eV) 75˚C to 150˚C	Activation Energy (eV) 175˚C to 325˚C
10	0.054	0.54
100	0.029	0.50
1000	0.14	0.46

spectroscopy is used to model the electrical properties of the material showing the presence of porous material, leakage capacitance and dominating grain response in the material. AC conductivity exhibits dispersion at low frequencies and follows Jonscher's power law. The change in the exponent n in ac conductivity dispersion term ($A\omega^n$) reveals the nature of conductivity mechanics. The conduction mechanism changes from localized hopping to free ion motion with increase in temperature and that the conduction is a thermally activated process.

5. Acknowledgements

PKB would like to acknowledge Department of Science & Technology, Government of India, New Delhi, for the grants received under FIST program and University Grants Commission, New Delhi for Major Research Project Grant No. F-16/24-2004

REFERENCES

[1] K. Brandt and A. Kemi, "X-Ray Studies on ABO_4 Compound Rutile Type and AB_2O_6 Columbite Type," *Mineral. Geol.*, Vol. 17A, No. 15, 1943.

[2] H. J. Goldschmidt, "An X-Ray Investigation of Systems between Niobium Pentaoxide and Certain Additional Oxides," *Metallurgia*, Vol. 62, 1960, pp. 211-218.

[3] F. Laves, G. Bayer and A. Panagos, *Schweiz Mineral Petrogr. Mitt.*, Vol. 43, 1963, p. 217.

[4] H. Brusset, R. Mahe and U. Aung Kyi, "Etude de niobates divalents binaires et ternaires a l'etat solide," *Materials Research Bulletin*, Vol. 7, No. 10, 1972, pp. 1061-1073. doi:10.1016/0025-5408(72)90158-4

[5] I. Yaeger, A. H. Morrish and B. M. Wanklyn, "Magnetization Studies in Transition-Metal Niobates: I. $NiNb_2O_6$," *Physical Review B*, Vol. 15, No. 3, 1977, pp. 1465-1476. doi:10.1103/PhysRevB.15.1465

[6] I. Yaeger, I. Maartense and B. M. Wanklyn, "Field-Induced Magnetic Transitions of $CoNb_2O_6$ in the Ordered State," *Solid State Communications*, Vol. 21, No. 1, 1977, pp. 93-96. doi:10.1016/0038-1098(77)91485-5

[7] I. Yaeger, A. H. Morrish, B. M. Wanklyn and B. J. Garrard, "Magnetization Studies in Transition-Metal Niobates. II. FeNb_ {2} O_ {6}," *Physical Review B*, Vol. 16, 1977, p. 2289. doi:10.1103/PhysRevB.16.2289

[8] K. N. Singh and P. K. Bajpai, "Synthesis, Characterization and Dielectric Relaxation of Phase Pure Columbite $MgNb_2O_6$: Optimization of Calcination and Sinterin," *Physica B*, Vol. 405, No.1, January 2010, pp. 303-312.

[9] H. Brusset, M. Gillier-Pandraud and S. D. Voliotis, "Etude de systemes binaires et pseudo-binaires definis entre Nb_2O_5 et PbO, SrO, BaO," *Materials Research Bulletin*, Vol. 6, 1971, p. 5.

[10] R. Roth, "Unit-cell Data of the Lead Niobate, $PbNb_2O_6$,"*Acta Crystallographica*, Vol. 10, No. 6, 1957, p. 437. doi:10.1107/S0365110X57001437

[11] H. J. Lee, K. S. Hong, S. J. Kim and I. T. Kim, "Effect of Vibro-Milling Time on Phase Formation and Particle Size of $ZnNbO_6$ Nano-Powders," *Materials Research Bulletin*, Vol. 32, No. 7, 1997, pp. 847-855. doi:10.1016/S0025-5408(97)00034-2

[12] R. C. Pullar, J. D. Breeze and N. Alford, "Characterization and Microwave Dielectric Properties of M2+ Nb_2O_6 Ceramics," *Journal of the American Ceramic Society*, Vol. 88, No. 9, 2005, pp. 2466-2471. doi:10.1111/j.1551-2916.2005.00458.x

[13] Y. C. Zhang, Z. X. Yue, Z. Gui and L. T. Li, *Material Letters*, Vol. 57, 2003, pp. 4531-4534.

[14] T. Kolodiazhnyi, A. Petric, A. Belous, O. V'yunov and O. Yanchevskij, "Synthesis and Dielectric Properties of Barium Tantalates and Niobates with Complex Perovskite Structure," *Journal of Materials Research*, Vol. 17, No, 12, 2002, pp. 3182-3189. doi:10.1557/JMR.2002.0460

[15] A. Ananta, R. Brydson and N. W. Thomas, "Synthesis, Formation and Characterisation of $MgNb_2O_6$ Powder in a Columbite-Like Phase," *Journal of the European Ceramic Society*, Vol. 19, No. 3, 1999, pp. 355-362. doi:10.1016/S0955-2219(98)00206-4

[16] N. Natarajan, V. Samuel, R. Pasricha, V. Ravi, "A Coprecipitation Technique to Prepare $BaNb_2O_6$," *Material Science & Engoneering B*, Vol. 117, No. 2, March 2005, pp. 169-171. doi:10.1016/j.mseb.2004.11.009

[17] V. Ravi, "A Coprecipitation Technique to Prepare $SrNb_2O_6$," *Material Characterization*, Vol. 55, No. 1, July 2005, pp. 92-95. doi:10.1016/j.matchar.2005.04.002

[18] K. S. Rao, P. M. Krishan, D. M. Prasad and J. H. Lee, "Influence of Samarium Substitution on Impedance Dielectric and Electromechanical Properties of $Pb_{(1-x)}K_{2x}Nb_2O_6$," *International Journal of Modern Physics B*, Vol. 21, No. 6, 2007, pp. 931-945. doi:10.1142/S0217979207036795

[19] K. S. Rao, D. M. Prasad, P. M. Krishna, B. H. Bindu and K. Suneetha, "Correlation between Low Frequency Dielectric Dispersion (LFDD) and Impedance Relaxation in Ferroelectric Ceramic $Pb_2KNb_4TaO_{15}$," *The Journal of Materials Science*, Vol. 42, 2007, p. 7363.

[20] L. Zhigao, J. P. Bonnet, J. Ravez and P. Hagenmuller, "Correlation between Low Frequency Dielectric Dispersion (LFDD) and Impedance Relaxation in Ferroelectric Ceramic $Pb_2KNb_4TaO_{15}$," *Solid State Ionics*, Vol. 57, No. 3-4, October 1992, pp. 235-244. doi:10.1016/0167-2738(92)90153-G

[21] T. A. Nealon, "Low-Frequency Dielectric Responses in PMN-Type Ceramics," *Ferroelectrics*, Vol. 76, 1987, pp. 371-382. doi:10.1080/00150198708016958

[22] A. K. Janscher, "The 'universal'dielectric response," *Nature*, Vol. 267, 1977, pp. 673-679. doi:10.1038/267673a0

[23] F. A. Kroger and H. J. Vink, "Relations between the Concentrations of Imperfections in Crystalline Solids," *Solid State Physics*, Vol. 3, 1956, pp. 307-435. doi:10.1016/S0081-1947(08)60135-6

[24] D. R. Chen and Y. G. Yen, *Electro. Elementary Math*, Vol. 1, 1982, p. 25.

[25] A. R. West, D. C. Sinclair, N. Hirose, "Characterization of Electrical Materials, Especially Ferroelectrics, by Impedance Spectroscopy," *The Journal of Electroceramics*. Vol. 1, No.1, 1975, pp. 65-71. doi:10.1023/A:1009950415758

[26] J. Ross Macdonald, "Impedance Spectroscopy: Emphasizing Solid Materials and Systems," Wiley Intersicence Publications, 1987.

[27] J. Maier, "The Polarization of Mixed Conducting SOFC Cathodes: Effects of Surface Reaction Coefficient, Ionic Conductivity and Geometry," *The Journal of the European Ceramic Society*, Vol. 24, No. 6, 2004, pp. 1343-1347.

[28] J. Maier, *Solid State Ionics*, Vol. 157, 2003, p. 327.

[29] A. K. Jonscher, "The 'universal'dielectric response," *Nature*, Vol. 267, 1977, pp. 673-679.

[30] D. C. Sinclair and A. R. West, "Impedance and Modulus Spectroscopy of Semiconducting $BaTiO_3$ Showing Positive Temperature Coefficient of Resistance," *Journal of Applied Physics*, Vol. 66, No. 8, 1989, pp. 3850-3857. doi:10.1063/1.344049

[31] I. M. Hodge, M. D. Ingram and Q. A. R. West, "Impedance and Modulus Spectroscopy of Polycrystalline Solid Electrolytes," *Journal of Electroanalytical Chemistry*, Vol. 74, No. 2, 1976, pp. 125-143. doi:10.1016/S0022-0728(76)80229-X

[32] A.K. Jonscher, "A New Understanding of the Dielectric Relaxation of Solids," *Journal of Materials Science*, Vol. 16, No. 8, 1981, pp. 2037-2060. doi:10.1007/BF00542364

